Magnetic, Kondo and non-Fermi-liquid behaviour of $U_{1-x}Th_xPd_2Al_3$

1999 J. Phys.: Condens. Matter 11 9775

(http://iopscience.iop.org/0953-8984/11/48/335)

J. Phys.: Condens. Matter **11** (1999) 9775–9796. Printed in the UK PII: S0953-8984(99)03025-8

Magnetic, Kondo and non-Fermi-liquid behaviour of $U_{1-x}Th_xPd_2Al_3$

Paul de V du Plessis†, André M Strydom†, Robert Troć‡, Tomasz Cichorek‡, Czesław Marucha‡ and Rachel P Gers†

† f-Electron Magnetism and Heavy-Fermion Physics Programme, Department of Physics, University of the Witwatersrand, Private Bag 3, PO WITS 2050, Johannesburg, South Africa

‡ W Trzebiatowski Institute for Low Temperature and Structure Research, Polish Academy of Sciences, 50-950 Wrocław, Poland

Received 26 March 1999, in final form 3 September 1999

Abstract. Electrical resistivity $\rho(T)$, magnetoresistance MR, magnetization $M(T, B)$ and magnetic susceptibility $\chi(T, B)$ measurements at temperatures down to 25 mK and applied magnetic fields up to 14 T are presented for Th-diluted $U_{1-x}Th_xPd_2Al_3$ alloys. For U-rich alloys, antiferromagnetic order is observed and T_N varies slowly with the Th concentration in the region $0 \leqslant x \leqslant 0.2$. From $\rho(T)$ data we calculate a value of the energy gap $\Delta = 12$ K in the spin-wave spectrum. In the U-rich concentration region a coherent Kondo description applies, but for alloys with $0.4 \leqslant x \leqslant 0.93$ a non-Fermi-liquid (NFL) phase prevails. An approximately linear temperature dependence of $\rho(T)$ is observed at low temperatures for about a decade in temperature, but deviation from this dependence occurs at the lowest temperatures. We show that the MR of the NFL alloys may be described in terms of the Coqblin–Schrieffer Hamiltonian, from which values of the single-ion characteristic Kondo temperature $T_K \approx 40$ K are calculated. An applied magnetic field is shown to recover Fermi-liquid dynamics in both $\chi(T)$ and $\rho(T)$. We give a description of the low-temperature magnetization $M(T, B)$ in terms of a two-channel Kondo model.

1. Introduction

The heavy-fermion (HF) compound UPd_2Al_3 exhibits the fascinating coexistence of magnetic order and superconductivity as is evidenced by bulk [1], neutron diffraction [2, 3] and muon spin-rotation [4, 5] measurements. Upon cooling, the material first orders at $T_N = 14.5$ K in an antiferromagnetic (AF) structure with spins aligned in the basal plane of the hexagonal $PrNi_2Al_3$-type crystal structure (space group $P6/mmm$) and with a magnetic wave vector $\boldsymbol{k} = [0, 0, \frac{1}{2}]$ [6]. With a further lowering of temperature it becomes superconducting at $T_{SC} = 1.8$ K while retaining its magnetic structure and ordered moment of $0.85\ \mu_B$/U [1, 2]. For polycrystalline UPd_2Al_3 the magnetic susceptibility $\chi(T)$ increases with decreasing temperature before reaching a broad maximum in $\chi(T)$ at about 35 K. For a single crystal this maximum is observed only for the basal-plane susceptibility $\chi_\perp(T)$ and is thought to originate from a special crystal-field level scheme with different Van Vleck contributions due to two low-lying singlets and the thermal populations of the excited singlet and doublet states [7]. A distinct change in slope of the $\chi(T)$ curve at a lower temperature indicates AF ordering at T_N. Single crystals of UPd_2Al_3 exhibit large anisotropy between the c-axis susceptibility $\chi_\parallel$ and the basal-plane susceptibility $\chi_\perp$ with $\chi_\perp \approx 4\chi_\parallel$ at 4 K [7]. The authors of reference [7] found for the magnetic field B applied within the basal plane that the magnetization curves exhibited small changes in slope at certain values of field. These and anomalies in $\chi(T)$, in

0953-8984/99/489775+22$30.00

$d\chi(T)/dT$, in magnetoresistance (MR) and in magnetostriction suggested a complex magnetic phase diagram with three different AF phases indicated for the field regime $0 \leqslant B \leqslant 5.5$ T. No corresponding anomalies were found with the field applied along the c-axis. Neutron diffraction studies however indicated that the intrinsic spin structure of UPd_2Al_3 is not altered by application of the magnetic field [3,8]. The neutron work associated the anomalies observed by the authors of reference [7] with reorientations of AF domains such that their moments are turned perpendicular to the applied-field directions within the basal plane [3, 8]. The specific heat of UPd_2Al_3 increases sharply upon cooling through T_N, and may be analysed in terms of a magnon contribution and a temperature-dependent, enhanced electronic contribution that extrapolates below T_N to $\gamma(0) = 150$ mJ mol^{-1} K^{-2} when $T \to 0$ [1]. This leads to an effective electron mass being nearly 70 times greater than that of the free-electron mass. It is further noted that a metamagnetic transition occurs at 1.3 K for a field of 18 T applied along the a-axis of single-crystal UPd_2Al_3. This transition is thought to be accompanied by the destruction of the HF state [9] and thereby modifies the carrier density. In recent years the solid solutions $U_{1-x}Th_xPd_2Al_3$ have also been intensively studied [10–14]. For these alloys with $0.4 \leqslant x \leqslant 0.95$ a non-Fermi-liquid (NFL) ground state has been indicated. Such a state has also been observed in several other cerium and uranium systems [11, 12]. NFL behaviour is characterized by a diverging electronic coefficient of the specific heat C in the limit $T \to 0$, often $\gamma(T) = C(T)/T \propto (-1/T_0)\ln(T/T_0)$, as well as a strong dependence of χ on temperature as $T \to 0$, e.g. $\chi(T) \propto 1-(T/T_0)^{1/2}$ [14]. These temperature dependences are observed at temperatures well below the characteristic scaling temperature T_0. In contrast to the preceding results, Fermi-liquid (FL) theory predicts constant values for the specific heat and susceptibility as $T \to 0$. The electrical resistivity of NFL materials is given by $\rho(T) = \rho_0 + aT^n$ where $a < 0$ or $a > 0$ and in many cases $n \approx 1$ rather than $n = 2$ as is expected for FL behaviour. NFL behaviour is often ascribed to the existence of a quantum critical point at zero temperature which may originate from fluctuations of an order parameter in the vicinity of an AF [15] or spin-glass phase transition [16] or is ascribed to the multichannel Kondo effect [17, 18]. On the other hand, in the NFL $UCu_{5-x}Pd_x$ system Cu NMR measurements [19] support the concept of Kondo disorder leading to a distribution of Kondo temperatures $T_K(T)$. A theory for Kondo disorder was presented by the authors of reference [19]. In recent studies the concepts of disorder and competition between RKKY and Kondo effects are proposed to lead to a Griffiths phase for which a simple power-law description for $C(T)/T$ and $\chi(T)$ is obtained [20]. Maple and co-workers [10–14] studied $C(T)$, $\chi(T)$ and $\rho(T)$ for a number of different alloys in the $U_{1-x}Th_xPd_2Al_3$ system. They analysed their data in terms of the above expressions for $C(T)/T$ and $\chi(T)$ and, by associating T_0 with the single-ion Kondo temperature T_K, they determined the dependence on the thorium concentration of T_K. They also indicate how T_N changes with Th dilution.

We present a study of the magnetization $M(T, B)$, $\chi(T, B)$ and $\rho(T, B)$ for the $U_{1-x}Th_xPd_2Al_3$ system which complements the work of Maple *et al* by giving *inter alia* a more complete phase diagram through studying more alloy compositions. We also extend the previous zero-field $\rho(T)$ studies of the above authors by presenting MR measurements for fields up to 14 T and for temperatures down to 25 mK. We indicate in an extension of our previous results [21] how the NFL behaviour of $\rho(T)$ is changed towards FL behaviour by application of such large magnetic fields. Our MR isotherms measured in fields up to 8 T are analysed in terms of the Bethe-*ansatz* solution of the Coqblin–Schrieffer Hamiltonian [22,23]. The resulting values of T_K are compared with those obtained by Maple *et al* from their zero-field measurements. Finally, $M(B)$ measurements are modelled by a two-channel Kondo description at low temperature [17, 18]. We also compare $\chi(T)$ with the results of Kondo-disorder models [24] as well as with a power-law prediction of Castro Neto *et al* [20].

2. Experimental details

Our polycrystalline $U_{1-x}Th_xPd_2Al_3$ samples were prepared using the following metals (given with their purities): 99.98 wt% U, 99.99 wt% Th, 99.97 wt% Pd and 99.999 wt% Al. The stoichiometric quantities of the elements for each composition were arc melted three times, with intermittent overturning of the ingot. The inside of the arc furnace was maintained at a slight underpressure of a titanium-gettered, high-purity argon atmosphere. The observed weight loss due to the melting process was in all cases less than 0.5 wt%. X-ray diffractograms establish that all alloys had the $PrNi_2Al_3$-type crystal structure, as well as establishing the absence of impurity phases within the experimental accuracy. Lattice parameters have been calculated using standard regression analyses on 13 well-resolved peaks in the powder spectrum of each alloy. Figure 1 depicts the dependence on the Th concentration of the hexagonal lattice parameters a and c, as well as the unit-cell volume. A linear increase in all three parameters with increase in Th content is evident. The solid lines in figure 1 represent iterated least-squares (LSQ) fits to the respective data sets and illustrate the validity of Vegard's law for this system.

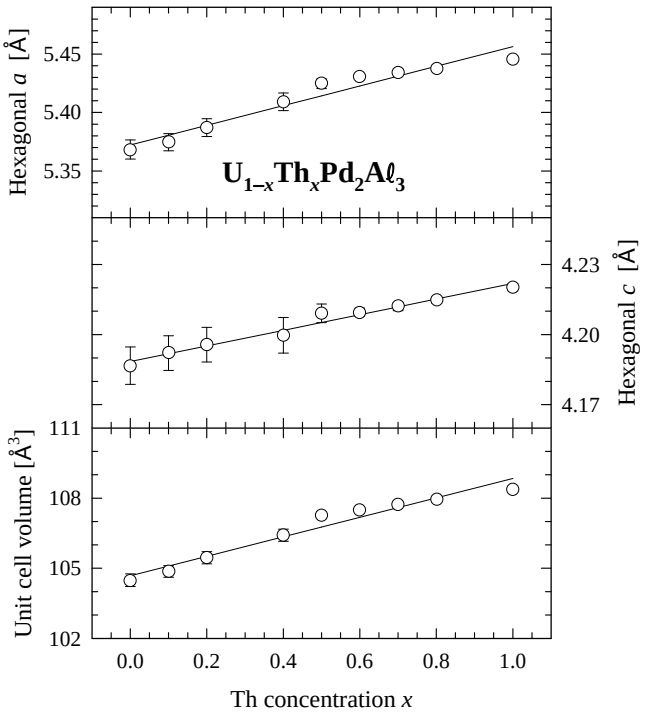

Figure 1. The dependence on the Th concentration of the hexagonal lattice parameters a and c, and of the crystallographic unit-cell volume for $U_{1-x}Th_xPd_2Al_3$.

For electrical transport studies, bars measuring typically $1 \times 1 \times 10$ mm^3 were cut from the ingots using spark erosion. The four-probe configuration was used for electrical measurements, and electrical contact to the specimens was established using spot welding. We used current reversal in an effort to eliminate spurious thermoelectric effects in the circuitry. For electrical measurements performed at the University of the Witwatersrand, a YEW-type 2854 dc source was used for the sample current, and the sample voltages were monitored with a Hewlett-Packard 3478A $5\frac{1}{2}$-digit multimeter. The magnetic field was obtained with an Oxford

Instruments superconducting magnet system and the field axis was positioned perpendicular to the current direction. Temperatures down to $T \approx 1.4$ K could be reached using an Oxford Instruments variable-temperature insert (VTI), and for measuring MR isotherms, we achieved a temperature stability of $T \pm 10$ mK for the duration of such an isotherm. The VTI was used together with an ITC[503] temperature controller. The sample temperatures were measured using calibrated carbon-glass and germanium resistive sensors and, in an applied field, a capacitive sensor. Sample temperatures down to 25 mK and in magnetic fields up to 14 T could be achieved for electrical transport measurements at the W Trzebiatowski Institute of Low Temperature and Structure Research of the Polish Academy of Sciences. For the magnetic susceptibility and magnetization measurements, also performed at the W Trzebiatowski Institute, samples were in the form of small, solid pieces of polycrystalline specimens. A Quantum Design SQUID magnetometer with a maximum field of 5 T and temperatures down to 1.7 K were used for these measurements.

3. Experimental results and discussion

3.1. Magnetization and susceptibility in the U-rich region

Measurements of the magnetization as a function of temperature and applied field were performed for the different $U_{1-x}Th_xPd_2Al_3$ alloys. An example of such a set of measurements for $U_{0.95}Th_{0.05}Pd_2Al_3$ is given in figure 2. For the U-rich compositions, the $M(B)$ curves are linear up to the maximum measuring field of 5 T used in our magnetization experiments.

Values of the susceptibility $\chi(T)$ measured in a field of 5 T are indicated in figure 3 for samples of different compositions. It is assumed that antiferromagnetic ordering sets in at temperatures determined by the inflection point ($d^2\chi(T)/dT^2 = 0$) on the $\chi(T)$ curves as indicated by arrows in figure 3. The Neél temperatures T_N thus determined are well

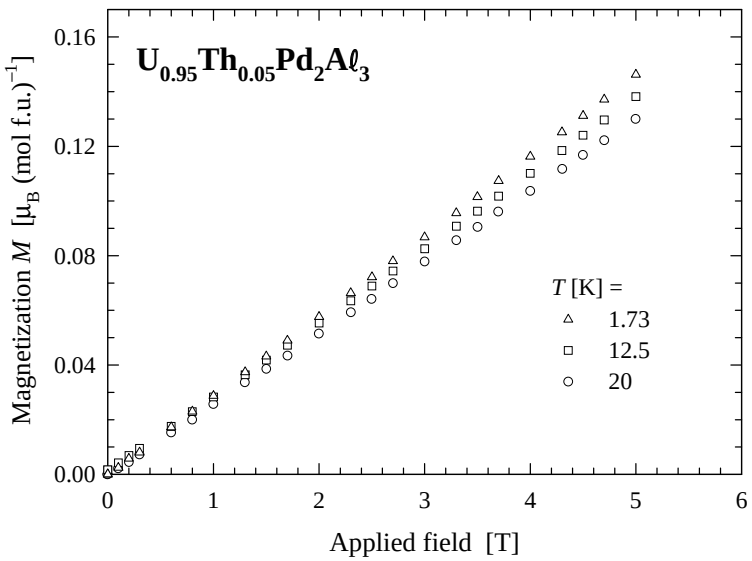

Figure 2. Magnetization isotherms for $U_{0.95}Th_{0.05}Pd_2Al_3$ at various temperatures. The magnetization measurements were performed during increasing and decreasing field sweeps and no hysteresis was evident from the results.

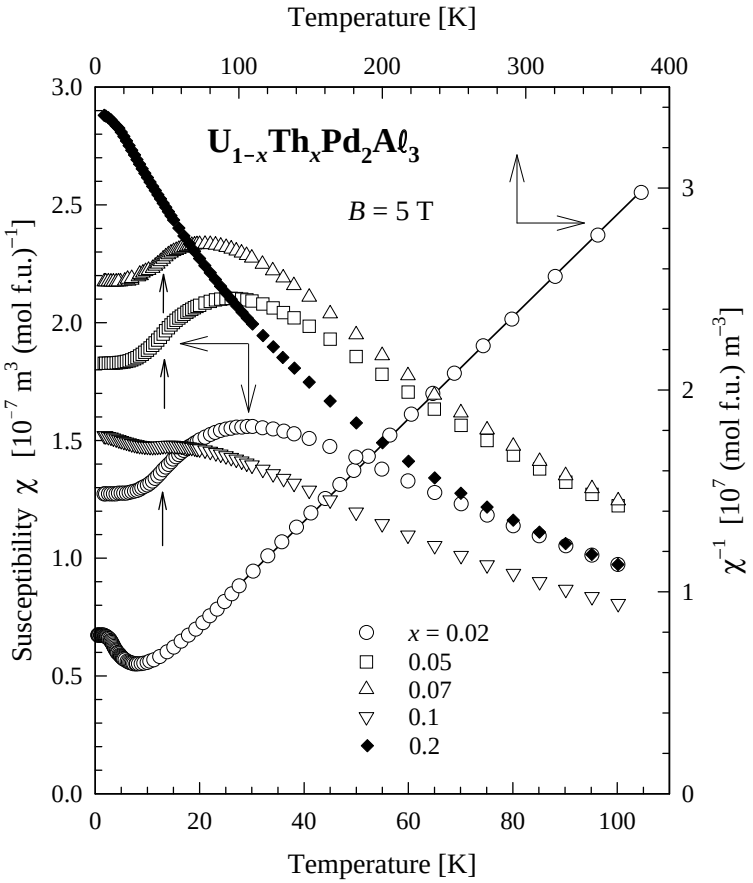

Figure 3. The temperature dependence of the magnetic susceptibility for $U_{1-x}Th_xPd_2Al_3$ alloys with $x \leqslant 0.2$ measured in a field of 5 T. A LSQ fit against a Curie–Weiss relation is indicated for the $x = 0.02$ composition.

below the broad maxima observed in $\chi(T)$ at temperatures T_{max}. These maxima have been ascribed either to short-range spin correlations [1] or to the crystal-field effect [7]. The concentration dependences of T_N and T_{max} will be discussed later, in section 3.2. Inverse magnetic susceptibility $\chi^{-1}(T)$ data for a representative sample are also shown in figure 3. The $\chi^{-1}(T)$ data are LSQ fitted for temperatures $T \geqslant 70$ K to a Curie–Weiss relation

$$\chi^{-1}(T) = \frac{3k_B(T - \theta_P)}{N_A\mu_{eff}^2} \tag{1}$$

where k_B is Boltzmann's constant and N_A is Avogadro's number. The dependences on the Th concentration of the paramagnetic Curie temperature θ_P and the effective paramagnetic moment μ_{eff} (per mol U) are displayed in figure 4. The dependences of θ_P and μ_{eff} on x are not explicitly given by Maple *et al* except for stating [10] that $\mu_{eff} = 3.24 \pm 0.06$ μ_B/mol U throughout the whole series and that θ_P fluctuates between -50 and -23 K. Our θ_P-values change monotonically from $\theta_P = -50$ K for UPd_2Al_3 to $\theta_P = -28$ K for the $x = 0.93$ compound. Concentration-independent values of μ_{eff} are observed over most of the composition range, except for a small decrease in μ_{eff} for the compositions with $x = 0.8$ and 0.93.

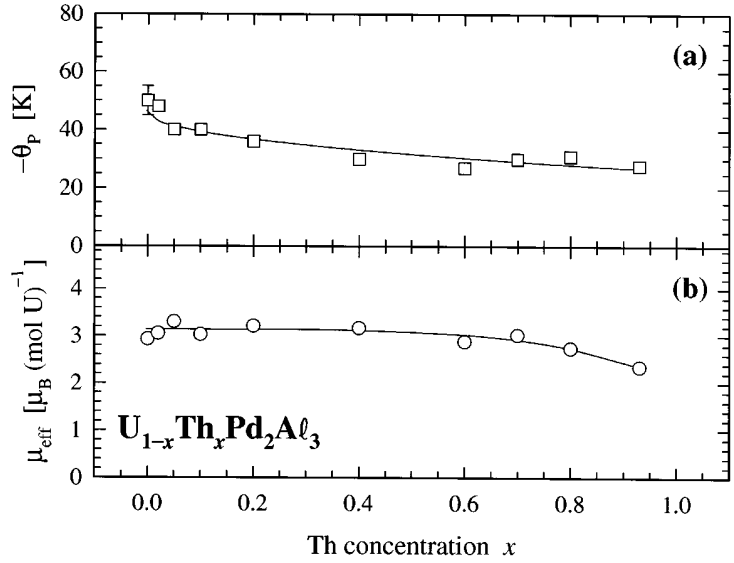

Figure 4. The dependence of (a) the paramagnetic Curie temperature $-\theta_P$ and (b) the effective paramagnetic moment μ_{eff} on Th concentration x for the $U_{1-x}Th_xPd_2Al_3$ alloys. The solid lines are guides to the eye.

3.2. Resistivity in the U-rich region

The $\rho(T)$ curves for UPd_2Al_3 and for $U_{1-x}Th_xPd_2Al_3$ ($0.05 \leqslant x \leqslant 0.2$) are depicted in figure 5. The qualitative behaviour for our UPd_2Al_3 sample is similar to results that appear in the literature for polycrystalline [1, 25], single-crystal [26, 27], and thin-film [28] UPd_2Al_3. The values of $\rho(T)$ observed by us are comparable to, albeit somewhat smaller than, those reported by most other groups. Figure 5 illustrates the remarkable sensitivity of $\rho(T)$ for small Th doping. This is an entirely new result that emerges from our studies [21] and which cannot be readily compared with those reported in previous work [10–14]. The latter report only relative results for $\rho(T)$, with data for different compositions normalized to the respective room temperature values. The reason for the dramatic increase in $\rho(T)$ with even a small Th doping of $x = 0.05$ is not clear at present.

The resistivity of UPd_2Al_3 is depicted for the antiferromagnetic region in figure 6. In the inset to figure 6 it is shown that a relatively large drop in $d\rho/dT$ takes place near 15 K. A similar drop in $d\rho/dT$ was observed by Sato *et al* [29] and they furthermore showed that it occurs at the temperature where the AF order parameter disappears as observed with neutron diffraction. Therefore the mid-point of this anomaly in $d\rho/dT$ is taken as indicative of T_N. It is noted that T_N indicated in this way occurs at a slightly lower temperature than that where the $\rho(T)$ curve appears to show a kink. Finally, after some precursor behaviour, our sample becomes superconducting at $T_{SC} = 1.5$ K.

The $\rho(T)$ results in the AF region have been fitted to the following equation:

$$\rho(T) = \rho_0 + \rho_{ph}(T) + bT\left(1 + \frac{2T}{\Delta}\right)\exp\left(-\frac{\Delta}{T}\right) + AT^2. \tag{2}$$

The first term in (2) indicates the defect and impurity scattering. The phonon contribution $\rho_{ph}(T)$ has been approximated by using the temperature-dependent part of our measured

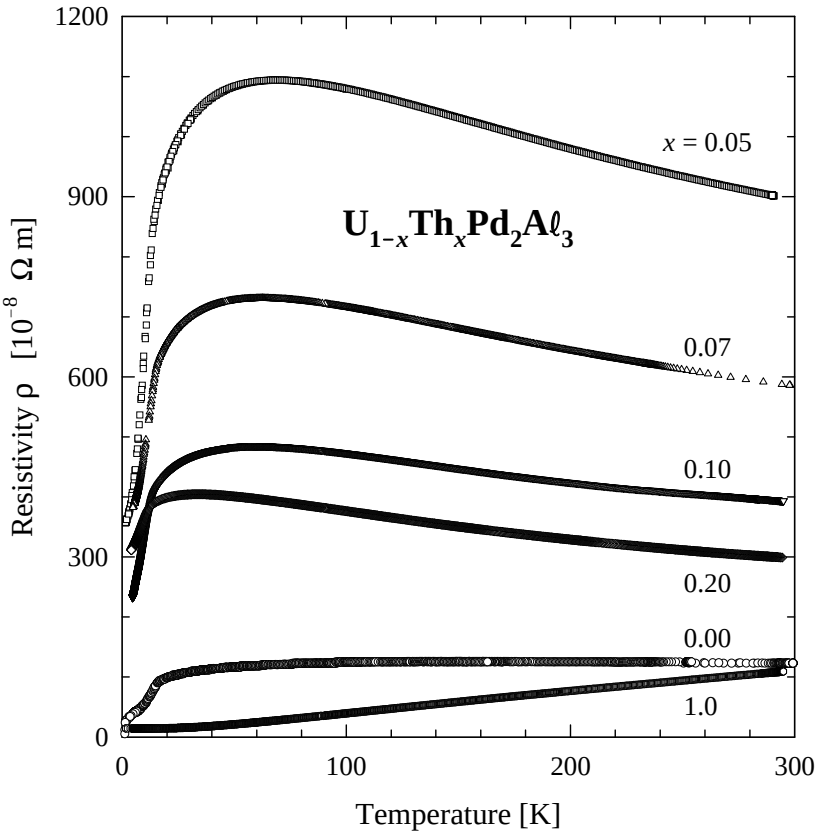

Figure 5. The temperature dependences of the electrical resistivity for uranium-concentrated compounds in the $U_{1-x}Th_xPd_2Al_3$ system ($0 \leqslant x \leqslant 0.2$), as well as for $ThPd_2Al_3$.

resistivity for the non-magnetic homologue $ThPd_2Al_3$ (see figure 5):

$$\rho_{\rm ph}(T) \approx \left[\rho(T) - \rho_0'\right]_{\rm ThPd_2Al_3} = \frac{4\kappa T}{\theta_{\rm R}^2}\left(\frac{T}{\theta_{\rm R}}\right)^4 \int_0^{\theta_{\rm R}/T} \frac{z^5\,{\rm d}z}{({\rm e}^z - 1)(1 - {\rm e}^{-z})}. \quad (3)$$

The LSQ parameters obtained by fitting the Grüneisen expression in (3) to the experimental data for $ThPd_2Al_3$ are $\theta_{\rm R} = 225 \pm 2$ K, $\kappa = (16\,880 \pm 20) \times 10^{-8}$ Ω m K and $\rho_0' = (14.48 \pm 0.05) \times 10^{-8}$ Ω m. These values of $\theta_{\rm R}$ and κ have been used to calculate $\rho_{\rm ph}(T)$ in (2). The third term in (2) is of spin-wave origin with Δ representing an energy gap in the antiferromagnetic spin-wave spectrum [30] and the last term gives a phenomenological Fermi-liquid quasiparticle excitation dependence. It should be noted that (2) was earlier used by other authors, but with the omission of $\rho_{\rm ph}(T)$, to fit the resistivity of UPd_2Al_3 and this resulted in values of $\Delta = 39$ K [27] and $\Delta = 40$ K [25]. Likewise omitting $\rho_{\rm ph}$(T) in our fit yields a value $\Delta = 36$ K which is in fair agreement with the previous studies. However, including $\rho_{\rm ph}(T)$ in (2), as is made possible by our measurements of $\rho(T)$ for $ThPd_2Al_3$, gives $\Delta = 12 \pm 4$ K. The remaining parameters are $\rho_0 = (35.7 \pm 0.5) \times 10^{-8}$ Ω m, $b = (1.06 \pm 0.06) \times 10^{-8}$ Ω m K^{-1} and $A = (0.11 \pm 0.05) \times 10^{-8}$ Ω m K^{-2}. An earlier inelastic neutron scattering experiment by Petersen *et al* [31] gave no evidence for a gap in the magnon spectrum to within an instrumental resolution of 4 K. Recent neutron scattering studies confirm the existence of a strongly damped spin wave [32] as earlier observed by Petersen *et al* ,

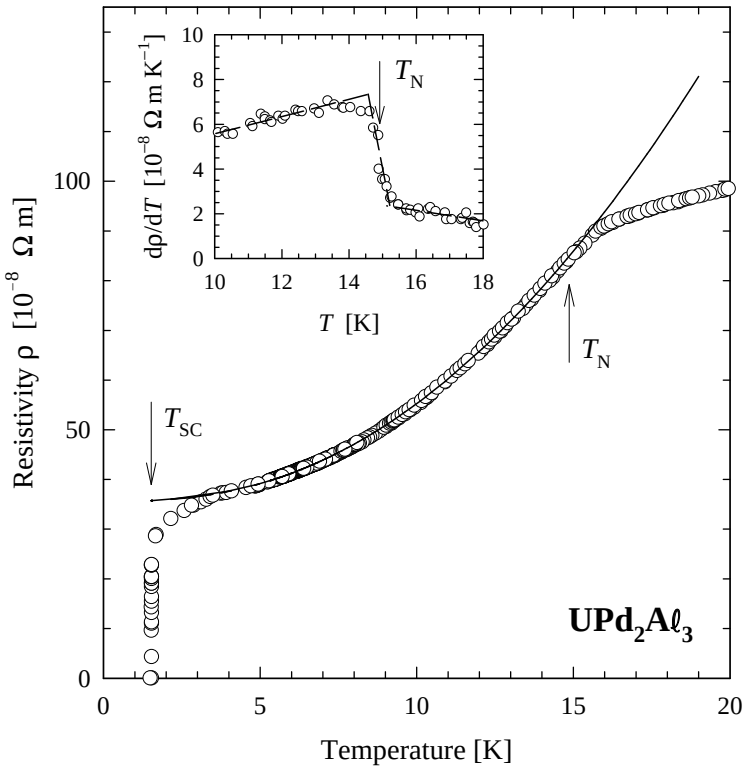

Figure 6. The temperature dependence of the electrical resistivity of UPd_2Al_3 at low temperatures. The solid line illustrates a LSQ fit of (2) to the data in the antiferromagnetic region. The inset indicates how T_N was determined from a plot of $d\rho(T)/dT$ versus T.

and furthermore indicate a spin-excitation gap ΔE_g associated with the superconducting phase which increases continuously from $\Delta E_g = 0$ to 4 K with decreasing temperature from T_{SC} down to 0.4 K [33]. In view of the considerably smaller gap found in our analysis as compared to previous results and the complicated neutron inelastic response observed, it seems worthwhile continuing such neutron studies, searching *inter alia* for a gap in the spin-wave response in the antiferromagnetic region above T_{SC}.

Values for T_N in the different $U_{1-x}Th_xPd_2Al_3$ alloys with $x \leqslant 0.1$ were determined in accordance with the criteria given by Sato *et al* [29]. The values thus obtained for T_N as a function of Th content are compared in figure 7(a) with T_N-values deduced from our $\chi(T)$ data. Fair agreement is observed between the two sets of data. Our results also confirm the report by Maple *et al* of a very gradual decrease in T_N with initial Th doping and the rapid disappearance of anomalies in $\rho(T)$ and $\chi(T)$ for compounds with $x \geqslant 0.2$. Values of T_{max} deduced from $\chi(T)$ for alloys with $x \leqslant 0.1$ are depicted in figure 7(b) and are observed to decrease more rapidly with x than is the case for $T_N(x)$. It would be of interest to determine how the magnetic order vanishes with increasing x using neutron diffraction measurements.

3.3. Resistivity and magnetoresistance in the non-Fermi-liquid region

Figure 8 illustrates the temperature dependence of $\rho(T)$ below room temperature for compositions with $0.4 \leqslant x \leqslant 1$. The measured $\rho(T)$ data have been normalized by

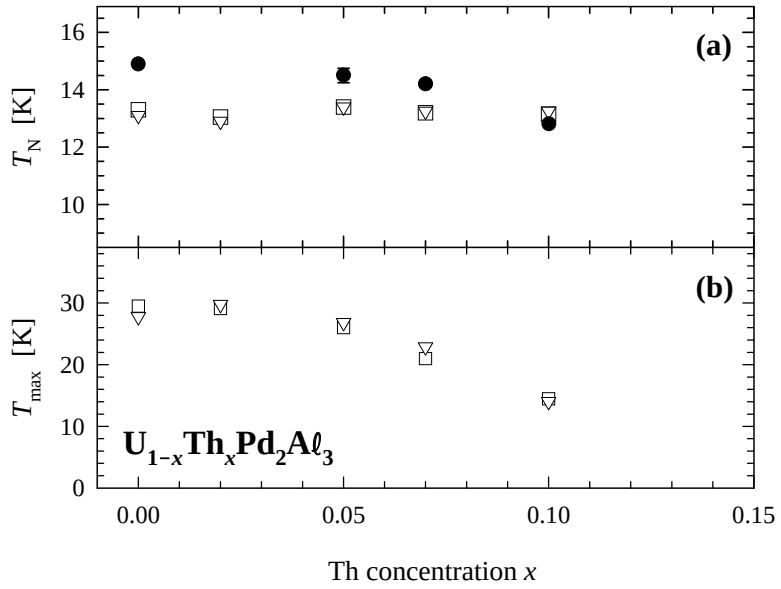

Figure 7. The dependences on the Th concentration of T_N, in (a), and of T_{max}, in (b), as obtained from $\rho(T)$ data (• symbols) and $\chi(T)$ data for $U_{1-x}Th_xPd_2Al_3$. The square symbols refer to $\chi(T)$ data taken in 5 T and the triangles to $\chi(T)$ data taken in 2 T.

plotting $\rho(T)/\rho(T = 295\ \mathrm{K})$ in order to negate differences in the disorder and static defect contributions. No cooperative effects, such as magnetic ordering which is innate to the $x \leqslant 0.2$ compositions, can be detected in $\rho(T)$ for the concentration range depicted in figure 8. For alloys with $x = 0.8$ and 0.93, a minimum in $\rho(T)$ is evident below room temperature due to the superposition of electron–phonon scattering which increases with temperature, and Kondo-type electron spin-flip scattering processes which decrease as they are driven off-resonance towards higher temperatures. In $U_{0.4}Th_{0.6}Pd_2Al_3$ and $U_{0.3}Th_{0.7}Pd_2Al_3$, $\rho(T)$ is dominated over a wide range of temperatures by a single-ion Kondo mechanism. $\rho(T)$ measurements for these two alloys have been extended to 600 K (not shown). Although the temperature coefficient of resistivity (TCR) becomes positive above room temperature for these alloys, there is still a change in the TCR at the highest measured temperatures, indicating that electron scattering by the U ions is still present at 600 K. In the inset to figure 8 the measured $\rho(T = 4\ \mathrm{K})$ are plotted as a function of Th concentration for the $x \geqslant 0.2$ alloys. A large enhancement occurs near $x = 0.5$ in accordance with the Nordheim rule [34].

The temperature dependences of the resistivity in zero field, and in magnetic fields up to 14 T applied perpendicular to the current direction in the sample, are shown in figure 9 for three $U_{1-x}Th_xPd_2Al_3$ alloys, namely for $x = 0.4$, 0.6 and 0.7. The data in figure 9 include measurements for decreasing and for increasing temperatures. No thermal hysteresis or remanence due to the magnetic field could be detected. For a magnetic impurity system, the single-ion Kondo theory predicts that conduction electron scattering increases with lowering temperature, but saturation behaviour is expected towards $T \to 0$ with formation of the singlet ground state of the magnetic ions. As shown in figure 9, such saturation behaviour in the zero-field measurements of $\rho(T)$ is observed for the $x = 0.4$ alloy and to a lesser extent the $x = 0.7$ alloy. However, in the case of the $x = 0.6$ alloy, the zero-field resistivity is not observed to level off in measurements down to $T = 1.5$ K. Very little curvature is observed below 20 K in

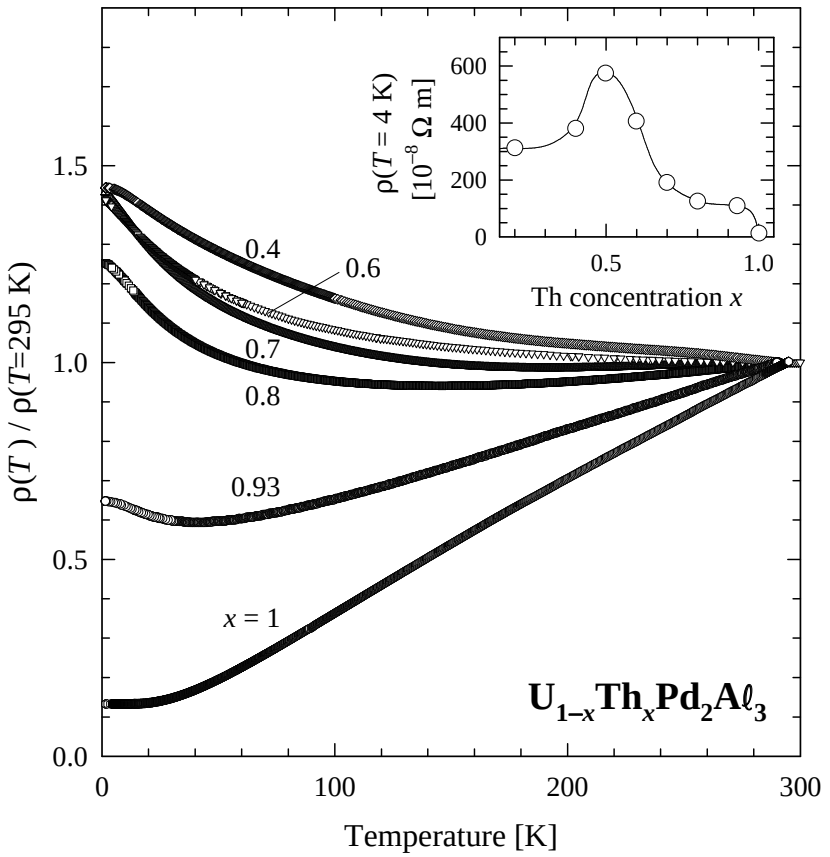

Figure 8. The temperature variation of the normalized electrical resistivity $\rho(T)/\rho(T = 295\ \mathrm{K})$ for uranium-dilute $U_{1-x}Th_xPd_2Al_3$ compounds. The inset plots the dependence on the Th concentration of $\rho(T = 4\ \mathrm{K})$.

this case, and a power-law fit of

$$\rho(T) = \rho(T = 0) + AT^n \tag{4}$$

with $n = 0.96 \pm 0.01$ and $A < 0$ accurately describes the data between 2 and 15 K. A large negative MR is evident for all of the alloys depicted in figure 9 resulting for the highest applied fields in the observation of a positive TCR at low temperatures. Two effects may contribute to a decrease in ρ for increasing fields at a given temperature: (a) the magnetic field could have an increasing alignment effect on the 5f moments, resulting in a decrease of the spin-disorder part of the total resistivity and hence elastic scattering, and (b) a freezing out of spin-flip scattering which decreases the inelastic scattering. It seems as if the latter mechanism is dominant in the present case since the large negative MR occurs only at low temperatures, $T \leqslant 30$ K.

In figure 10 a double-$\log_{10}$ plot is used to indicate the temperature regime over which a power-law fit according to (4) of the data is adhered to for the $x = 0.6$ sample in $B = 0$ and for the $x = 0.4$, 0.5, 0.6 and 0.7 samples in $B = 14$ T. A plot of $\mp\{\rho(T, B) - \rho(0, B)\}$ versus T^n is given with n obtained by a LSQ fit of each set of data. The $-$ sign refers to the $B = 0$ data (negative TCR) and the + sign to the various sets of data for $B = 14$ T (positive TCR). We note that an ≈15% drop in the zero-field $\rho(T)$ was observed for the $x = 0.6$ sample below

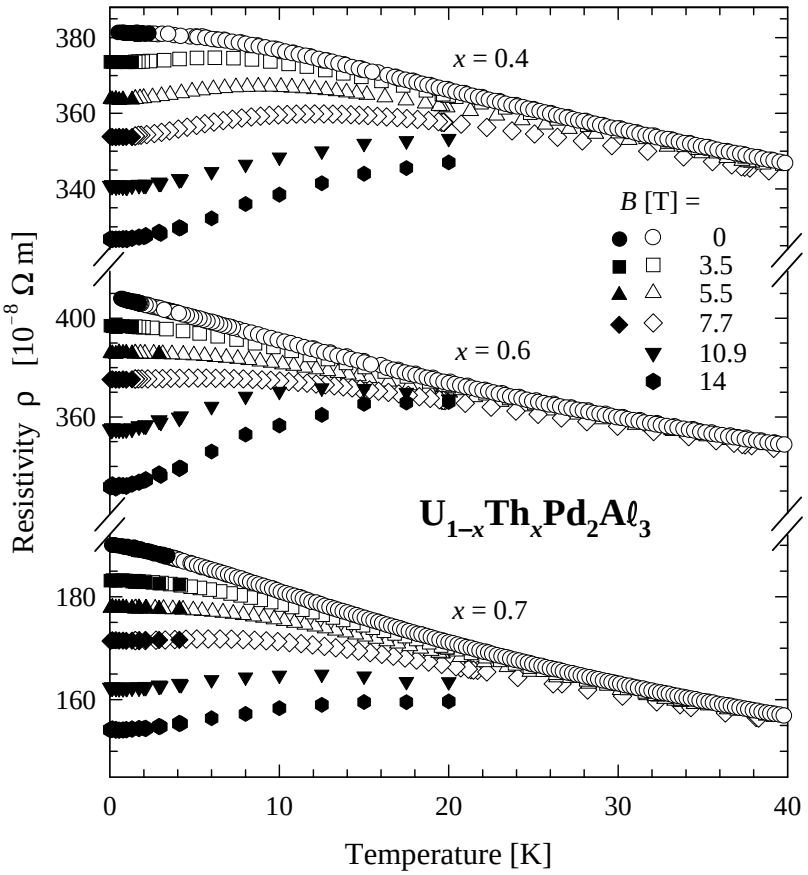

Figure 9. The effect of various magnetic field strengths (perpendicular to the direction of the current) on the temperature dependence of the electrical resistivity $\rho(T)$ for three alloys in the system $U_{1-x}Th_xPd_2Al_3$. Data points represented with open symbols were measured at the University of the Witwatersrand and those with filled symbols at the W Trzebiatowski Institute. This convention will also be followed in figures 10, 11 and 14 where resistivity data measured in both laboratories are depicted.

500 mK (not shown in figure 10). This drop in $\rho(T)$ is ascribed to the superconductivity of a small amount of a spurious phase in the sample. The small circle symbols superimposed onto the zero-field data in figure 10 represent data measured in a field of 1 T which proved to sufficiently erase the small anomaly in $\rho(B = 0)$ found in this alloy. We have observed a similar effect (but at a higher temperature of 4 K) in U_2Fe_2Sn and have shown that it was caused by a small amount of Sn that precipitated on the grain boundaries of the material [35]. Values of $\rho(0, B)$, A and n obtained from the LSQ fits are given in table 1 together with the range of validity of the power-law description (4). It is observed that the data for the $x = 0.6$ alloy in $B = 0$ deviate from the indicated $T^{0.96}$-dependence below 2 K. Similar and larger deviations occurred for the $B = 0$ results for the other alloys and this will be discussed below (figure 14). The results for the various alloys in an applied field of $B = 14$ T indicate a clear tendency of recovery of FL behaviour. However, it is noted from the observed values of n, especially for the $x = 0.6$ alloy, that the 14 T field is still not large enough to completely establish the FL state.

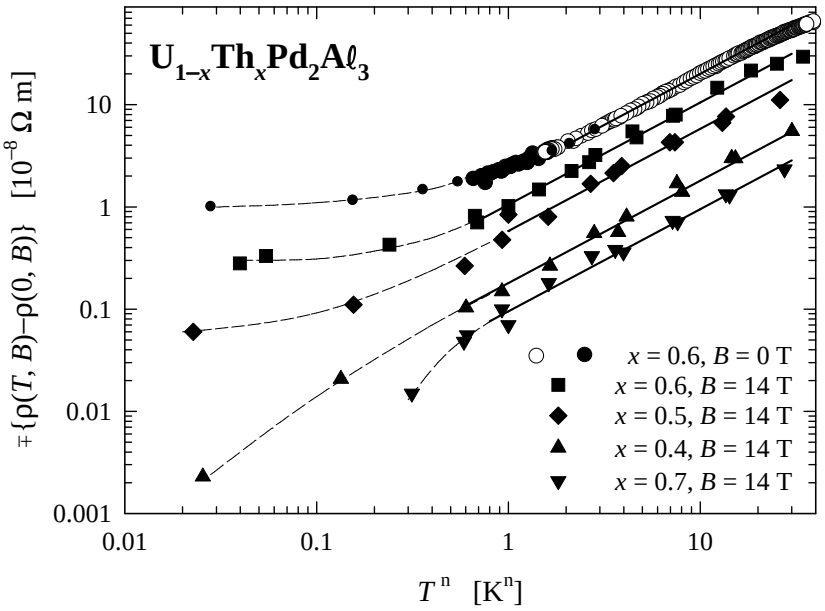

Figure 10. A double-$\log_{10}$ plot of the temperature-dependent part $\mp\{\rho(T, B) - \rho(0, B)\}$ of the electrical resistivity as a function of T^n for various NFL $U_{1-x}Th_xPd_2Al_3$ alloys. The solid lines are LSQ fits to the respective data sets (see table 1 for the fit parameters and ranges) and the dashed lines are guides to the eye. The $-$ sign refers to results for $B = 0$ T and the + sign for data taken in $B = 14$ T.

Table 1. The LSQ fit parameters for the compounds $U_{1-x}Th_xPd_2Al_3$, $x = 0.4$, 0.5, 0.6 and 0.7, describing the electrical resistivity (see figure 10) according to (4) for zero applied field and for 14 T.

Th concentration x	Field (T)	$\rho(0, B)$ (10^{-8} Ω m K)	A (10^{-8} Ω m K^{-n})	n	Range of fit (K)
0.6	0	409.7 ± 0.7	-2.00 ± 0.05	0.96 ± 0.01	$2 \leqslant T \leqslant 20$
0.6	14	326.5 ± 0.7	1.05 ± 0.05	1.40 ± 0.05	$0.78 \leqslant T \leqslant 10$
0.4	14	326.8 ± 0.1	0.18 ± 0.02	1.90 ± 0.05	$0.76 \leqslant T \leqslant 6.0$
0.5	14	573.0 ± 0.4	0.58 ± 0.02	1.82 ± 0.08	$1.0 \leqslant T \leqslant 3.9$
0.7	14	154.2 ± 0.3	0.095 ± 0.009	1.85 ± 0.05	$0.76 \leqslant T \leqslant 3.8$

The deviations from a power-law fit of the various curves in $B = 14$ T in figure 10 at the lowest temperatures are of the order of the experimental measuring and extrapolation uncertainties. At higher temperatures ($\sim$20 K) the curves deviate because a peak in the resistivity develops. This is illustrated for the $U_{0.4}Th_{0.6}Pd_2Al_3$ alloy in figure 11 where the maxima in $\rho(T, B)$ for $B = 7.7$, 10.9 and 14 T are indicated by arrows. This illustrates how the application of the magnetic field induces Kondo-lattice behaviour in our system. The shift of the maximum in $\rho(T, B)$ to higher temperatures for larger applied fields is in agreement with theoretical expectations [36] and previous experimental studies [37].

Isothermal MR measurements taken in fields up to 8 T have been performed for the samples with $0.4 \leqslant x \leqslant 1$ and as an example the results for $U_{0.4}Th_{0.6}Pd_2Al_3$ are given in figure 12. For the analyses of our MR data described below, we approximate the U contribution $[\rho(T, B)/\rho(T, 0)]_{5f}$ to the total measured MR for each isotherm by subtracting

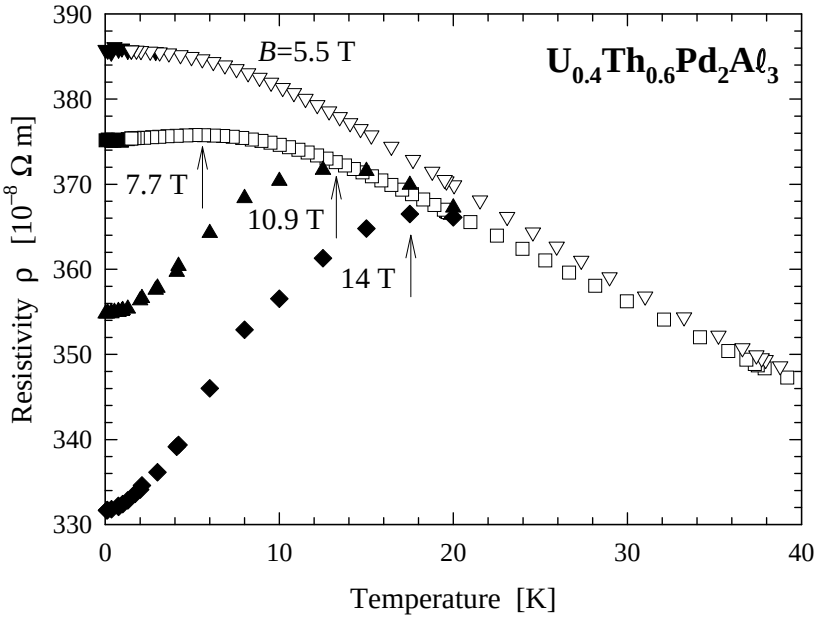

Figure 11. The effect of various magnetic field strengths (perpendicular to the direction of the current) on the temperature dependence of the electrical resistivity $\rho(T)$ for $U_{0.4}Th_{0.6}Pd_2Al_3$. The arrows indicate the positions of observed maxima in $\rho(T, B)$.

the MR measured for $ThPd_2Al_3$ at the corresponding temperature. From the perspective of the single-ion Kondo interpretation for certain properties of the $U_{1-x}Th_xPd_2Al_3$ system, the MR data were fitted to the calculations of MR obtained for the Bethe-*ansatz* solution of the Coqblin–Schrieffer Hamiltonian in the integer-valence limit [22, 23]. The resistivity in a field is given by

$$\rho(B) = \rho(B=0)\cos^2\frac{\pi}{2}M_{\rm I}(B). \tag{5}$$

Both the magnetization and the MR can be expressed in terms of the occupation numbers n_l of the f levels. For $j = \frac{1}{2}$ in the integer-valence limit it follows that

$$\frac{\rho(B=0)}{\rho(B)} = \frac{1}{2j+1}\sin^2\left[\frac{\pi n_{\rm f}}{2j+1}\right]\sum_{l=0}^{2j}\sin^{-2}(\pi n_l) \tag{6}$$

with

$$\sum_{l=0}^{2j} n_l = n_{\rm f} = 1.$$

The magnetic field dependence of the resistivity was found by calculating the impurity magnetization $M_{\rm I}$ over the various field ranges given by Andrei *et al* [38]. Justification for using $j = \frac{1}{2}$ for the ground state of UPd_2Al_3 is based on specific heat [11], neutron scattering [2] and Hall-effect [39] results. We assume that $j = \frac{1}{2}$ will also be appropriate for the Th-substituted derivatives of UPd_2Al_3.

The results of LSQ fits to (6) are given as solid lines in figure 12. Relatively good fits of the experimental data points are evident at higher temperature, but the fits become progressively worse for the lowest temperatures. Our treatment of the MR data assumes that the total effect of

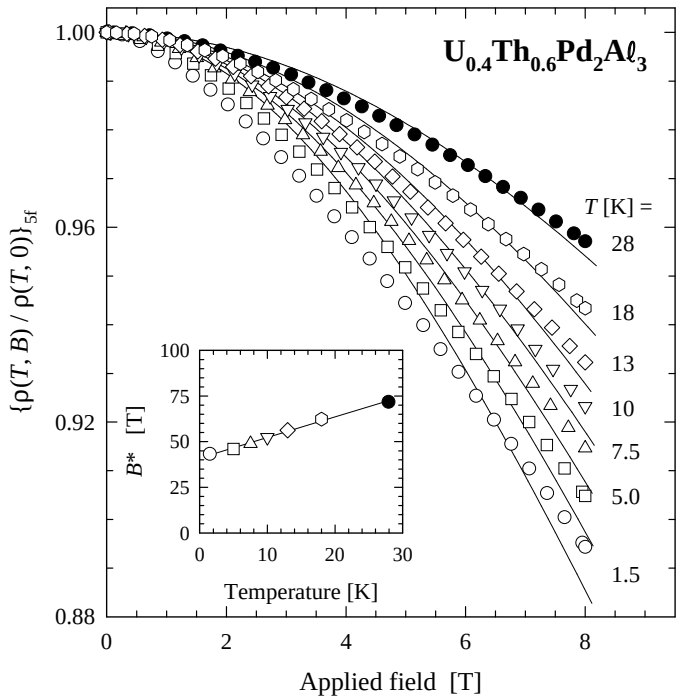

Figure 12. The isothermal magnetic field dependences of the 5f-derived normalized electrical resistivity $\{\rho(T,B)/\rho(T,0)\}_{5f}$ for $U_{0.4}Th_{0.6}Pd_2Al_3$ at various temperatures. The magnetoresistance contribution of the non-magnetic $ThPd_2Al_3$ homologue has been subtracted from all of the isotherms. Measurements were performed with increasing fields and followed by decreasing field scans. The solid lines illustrate LSQ fits of (6) to the data yielding, for each isotherm, a characteristic field $B^*(T)$ which is plotted (symbols corresponding to isotherms in the main graph) and LSQ fitted (solid line) in the inset according to (7). The fit parameters for the various alloys are given in table 2.

Table 2. Values of the Th-concentration-dependent parameters T_K and μ_K as obtained from magnetoresistance (MR) measurements, and the power-law index n and LSQ fitting range pertaining to zero-field $\Delta\rho(T,0)$ data (see figure 14) fitted to (8) for samples in the NFL region of $U_{1-x}Th_xPd_2Al_3$.

	MR		$\Delta\rho(T,0)$	
Th concentration x	T_K (K)	μ_K (μ_B)	n	Fitting range (K)
0.4	41 ± 1	0.74 ± 0.01	0.95 ± 0.01	$12 \leqslant T \leqslant 62$
0.5	42 ± 1	0.76 ± 0.01	0.97 ± 0.01	$9 \leqslant T \leqslant 25$
0.6	37 ± 1	0.66 ± 0.02	0.97 ± 0.01	$3 \leqslant T \leqslant 20$
0.7	35 ± 1	0.69 ± 0.01	0.99 ± 0.01	$14 \leqslant T \leqslant 35$

the field on the resistivity originates in the single-ion Kondo mechanism, and negates possible cooperative effects such as interuranium interactions which evidently become more important at low temperatures. In spite of this caveat, it is observed below that the LSQ fits of the lowest-temperature isotherms also give results that conform to the single-ion expectations. Consequently, we also include these fits in figure 12. From the LSQ fit results, one can derive

values of the characteristic field $B^*(T)$. According to Batlogg *et al* [40]

$$B^*(T) = B^*(0) + \frac{k_B T}{g\mu_K} = \frac{k_B}{g\mu_K}(T_K + T) \tag{7}$$

with g the Landé factor and μ_K the effective moment of the Kondo ion. The result of a LSQ fit of (7) to the $B^*(T)$ data (see the inset to figure 12) leads to values of $T_K(x)$ and $\mu_K(x)$ as given in table 2. These values, together with $B^*(0)$ for each alloy, are plotted in figure 13. Our MR-derived values of $T_K(x)$ are 60% larger than the values obtained from $C(T)$ and $\chi(T)$ by Maple *et al* [11]. This presents satisfactory agreement for the parameter T_K that is known to depend somewhat on the experimental probe used for its determination. In both studies an enhancement is observed in the value of T_K towards the uranium-dilute limit. Furthermore, we find μ_K to be approximately constant for the NFL alloys.

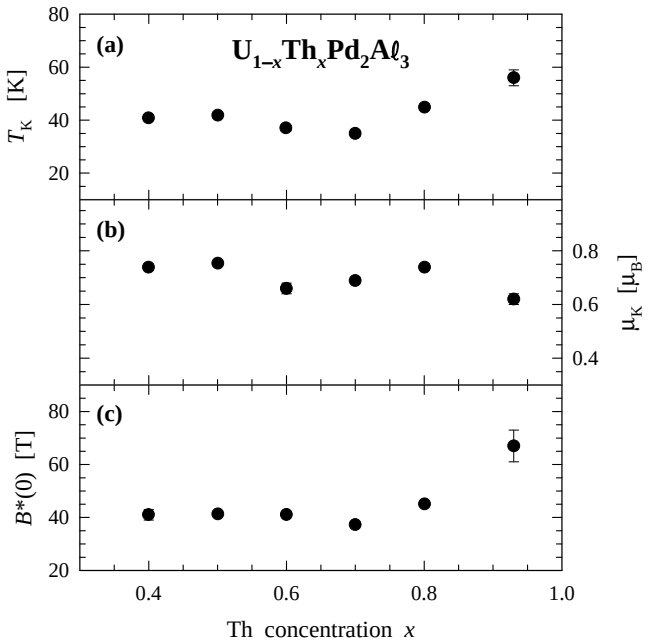

Figure 13. The dependence on the thorium concentration of parameters obtained using the Bethe-*ansatz* description of the magnetoresistance: (a) the single-ion Kondo temperature T_K, (b) the Kondo-ion magnetic moment μ_K and (c) the characteristic field $B^*(0)$.

The 5f contribution to the measured resistivity for NFL $U_{1-x}Th_xPd_2Al_3$ alloys, $\Delta\rho(T)$, has been described [12] in terms of a scaling relation

$$\frac{\Delta\rho(T)}{\Delta\rho(0)} = 1 - a\left(\frac{T}{T_K}\right)^n. \tag{8}$$

In (8), $\Delta\rho(T)$ is calculated for each composition by subtracting the resistivity of $ThPd_2Al_3$, $\rho_{Th}(T)$, from the measured $\rho(T)$. $\rho(T)$ data for the non-magnetic homologue $ThPd_2Al_3$ (figure 5) were LSQ fitted against the Grüneisen expression (3) and the values of θ_R and κ thus obtained were used to subtract $\rho_{ph}(T)$ from the measured $\rho(T)$ for the various alloys in order to obtain the 5f contribution to their resistivities. Plots of $1 - \Delta\rho(T)/\Delta\rho(0)$ versus T/T_K are given in figure 14 for alloys with $x = 0.4$, 0.5, 0.6 and 0.7. The values of T_K that were used for each compound were obtained from calculations of the field dependence of the resistivity.

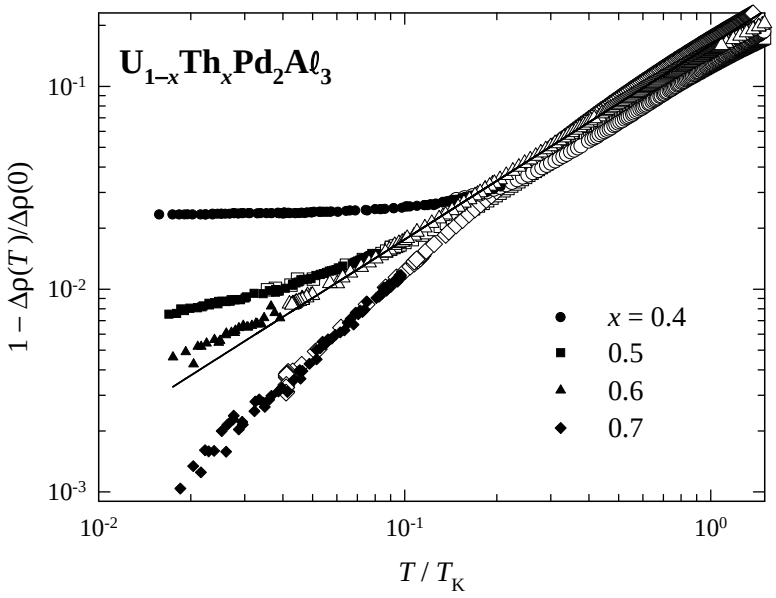

Figure 14. The T_K-scaled temperature dependence of the reduced resistivity (see the text) in a double-$\log_{10}$ plot. The open symbols represent data measured at the University of the Witwatersrand and extend down to 1.4 K. Lower-temperature data were measured in Wrocław. The solid line superimposed onto the $x = 0.6$ data is a LSQ fit according to (8). The power-law indices n and fitting ranges for the various alloys are given in table 2.

On the other hand, in the analysis by Maple *et al* [12] the value of the prefactor a in (8) was adjusted in order to make their ρ-derived values of T_K agree with those obtained from their specific heat measurements.

The representation in figure 14 expresses the evolution in the behaviour of $\rho(T)$ below T_K. The data at higher temperatures can be fitted for all alloys to the scaling relation (8). For instance, for the $x = 0.6$ alloy, a LSQ fit of (8) with $T_K = 37.0$ K (shown as a solid line in figure 14) to the data yields $a = 5.11 \pm 0.07$ and $n = 0.97 \pm 0.01$ over the temperature range $3 \leqslant T \leqslant 20$ K. It is noted that this value for n obtained using a correction pertaining to $\rho_{Th}(T)$ is, within the error, of the magnitude of the value $n = 0.96 \pm 0.01$ (see table 1, figure 10) that was obtained by ignoring the non-f-electron contribution to the electrical resistivity which is evidently small at low temperatures. It is evident for this alloy, and also more pronouncedly for the other alloys, that there is a departure from the NFL description at the lowest temperatures. This has also been observed by Maple *et al* [11, 12]. The results in figure 14 suggest that it may be possible, by tuning x between 0.6 and 0.7, to extend the occurrence of a linear 5f electrical resistivity to very low temperatures. Values of n, together with the fitting range of temperatures used in analysing the results of figure 14 for several NFL alloys, are given in table 2.

3.4. Magnetization and susceptibility in the non-Fermi-liquid region

Magnetization isotherms for a representative NFL sample ($x = 0.7$) are given in figure 15. It is observed that the M-versus-B data at low temperatures display negative curvature. This behaviour is in clear contrast with low-temperature magnetization isotherms measured for antiferromagnetic $U_{1-x}Th_xPd_2Al_3$ alloys which show linear M-versus-B curves up to 5 T as

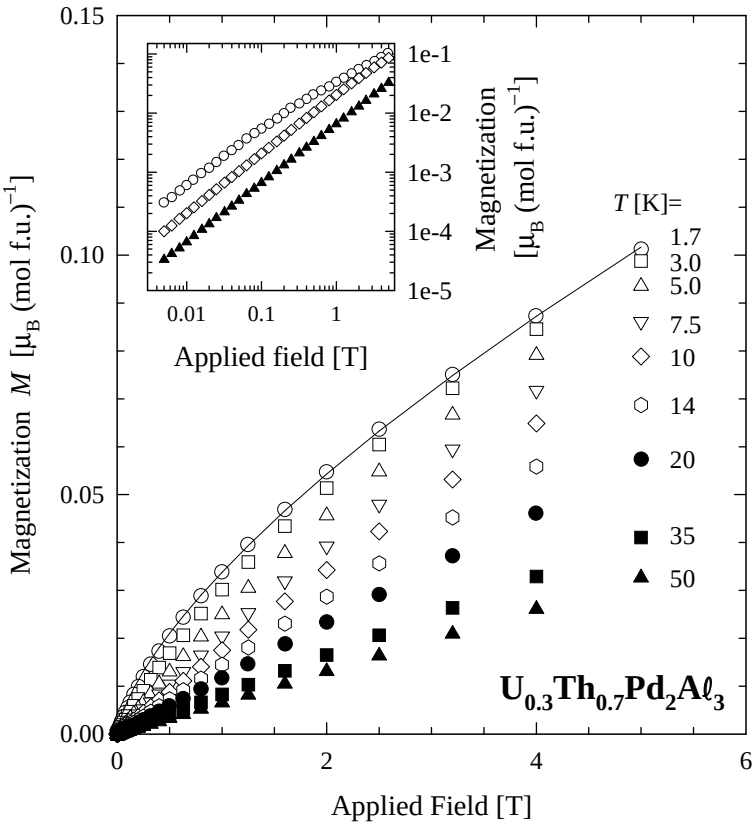

Figure 15. Magnetization measurements for $U_{0.3}Th_{0.7}Pd_2Al_3$ at various sample temperatures. The solid line is a fit of the power law (9) to the $T = 1.7$ K data and gives an exponent $\eta = 2.92 \pm 0.02$. The inset illustrates the low-field data in a double-$\log_{10}$ plot.

illustrated in figure 2. Such non-linear magnetization curves seem to be a feature of not only the $U_{1-x}Th_xPd_2Al_3$ system [41, 42], but also other NFL systems (e.g. $U_{1-x}Y_xPd_3$ [11, 41, 45, 46], $UCu_{5-x}Pd_x$ [19, 46–49], UBe_{13} [43], $U_{1-x}Th_xBe_{13}$ [44] and $CeCu_{6-x}Au_x$ [50]). In the case of $U_{1-x}Y_xPd_3$ and $UCu_{5-x}Pd_x$ the curvature has been ascribed to an impurity contribution which was subtracted from the raw data to yield the intrinsic susceptibility values [11, 45, 46]. In the following we rather consider the total measured susceptibility as intrinsic. Firstly, it is noted that the magnetization curves in figure 15 cannot be explained in terms of the thermal fluctuations of a free spin. It may readily be verified that a presentation of the M-versus-B/T low-temperature data from figure 15 does not yield a universal Brillouin function. One rather deals with a strongly correlated system with moments suppressed by the Kondo interaction. In the following we attempt to interpret the magnetization and susceptibility in terms of an application of the multichannel Kondo model [17, 18, 51].

NFL behaviour is obtained for the overcompensated multichannel Kondo model with the number of conduction electron channels $\eta > 2S_I$, where S_I is the impurity spin. The Bethe-*ansatz* solution for $S_I = \frac{1}{2}$, $\eta > 2S_I$ yields a power-law relation for the field dependence of the zero-temperature, low-field magnetization [17, 18]:

$$M_{\eta>2S_I} = b\left(\frac{\mu_B B}{k_B T_K}\right)^{2/\eta}. \tag{9}$$

The particular case of the two-channel Kondo model $\eta = 2$ and with $S_I = \frac{1}{2}$ has been argued to be applicable to several rare-earth and actinide NFL systems. In this case a logarithmic divergence is obtained for the field-dependent magnetization:

$$M_{\eta=2S_I} = c\left(\frac{\mu_B B}{k_B T_K}\right) \ln\left(\frac{\mu_B B}{k_B T_K}\right). \tag{10}$$

The data points shown in the main part of figure 15 have been fitted for each isotherm against the power law (9). A value of $\eta = 2.92 \pm 0.02$ is obtained for the 1.73 K isotherm and the corresponding fit is given as a solid line. For the 20 K isotherm the M–B curve is almost linear and a value of $\eta = 2.03 \pm 0.01$ is observed. We have also performed measurements in the low-field regime down to $B = 0.005$ T and three of these isotherms are displayed as a double-$\log_{10}$ plot in the inset to figure 15. It is observed that upon decreasing B the slope of a line that may be fitted say through the 1.73 K isotherm gradually changes until it reaches a constant value for the field regime $0.005 \leqslant B \leqslant 0.1$ T. This constant slope yields a value $\eta = 2.01$. The power-law description (9) is valid only for $\eta > 2$ and therefore the observed magnetization results suggest that the data should be fitted against (10) which describes the $\eta = 2$, $S_I = \frac{1}{2}$ case. In figure 16 it is indicated that good fits of our data are obtained against the two-channel Kondo expression for the magnetization for $0.005 \leqslant B \lesssim 0.13$ T and for isotherms with $1.7 \leqslant T \leqslant 50$ K. A value for the Kondo temperature of $T_K = 35$ K found from the MR analysis was used. It is noted that Maple *et al* [12] analysed their specific heat data for this system using a theoretical description for the two-channel spin-$\frac{1}{2}$ Kondo model.

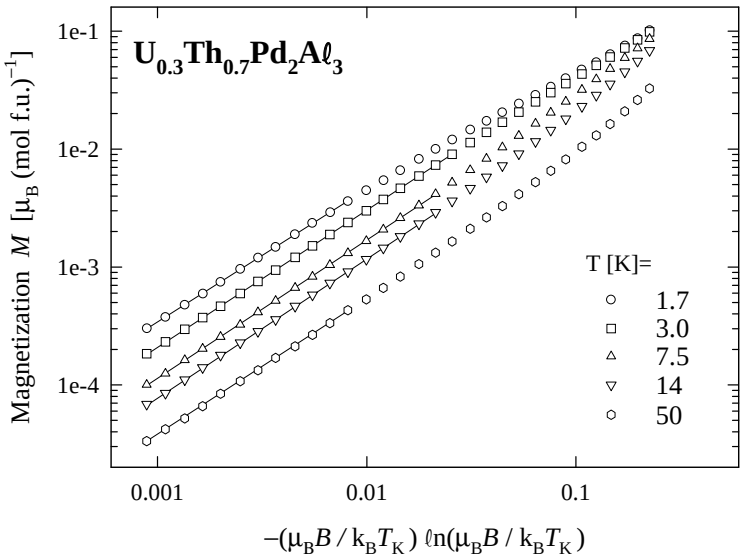

Figure 16. Magnetization isotherms plotted against the product function $(-\mu_B B/k_B T_K) \times \ln(\mu_B B/k_B T_K)$ in order to test the two-channel Kondo expression in (10). The LSQ solid lines indicate the range in magnetic field for which (10) provides a suitable description of the experimental data points.

We also attempted to fit the results of figure 15 in terms of first- and third-order susceptibility terms (χ_1, χ_3) in the following expression [52]:

$$M = \chi_1 B + \frac{1}{3!}\chi_3 B^3 + \cdots. \tag{11}$$

The resulting fit was unsatisfactory and hence a description in terms of the temperature dependence of χ_3 as given for the proposed quadrupolar Kondo state in the $U_{1-x}Th_xBe_{13}$ system [43, 44] cannot be given in our case.

Maple *et al* [14] observed the following temperature dependence for the susceptibility in the NFL region of the $U_{1-x}Th_xPd_2Al_3$ system in the low-temperature limit:

$$\frac{\chi(T)}{\chi(0)} = 1 - g\left(\frac{T}{T_K}\right)^{1/2}. \tag{12}$$

We also found that our alloys in the NFL region scale reasonably well to (12) using our MR-derived values of T_K for each alloy. In figure 17 we present our susceptibility M/B data for $U_{1-x}Th_xPd_2Al_3$ ($x = 0.7$, 0.8) measured for different values of applied field varying from $B = 5$ T to 0.008 T. It is observed that in the limit of low fields the results indicate a power-law behaviour, $\chi(T) \sim T^{-m}$, for both alloys over more than a decade in temperature. Values of the exponents $m = 0.655 \pm 0.005$ for $x = 0.7$ and $m = 0.580 \pm 0.005$ for $x = 0.8$ are obtained. In the low-temperature limit in sufficiently high fields the susceptibility becomes temperature independent as is to be expected for the Fermi-liquid ground state which is obtained as the channel degeneracy is lifted [18].

In a recent theoretical study, Castro Neto *et al* [20] proposed a model that is based upon the proximity to a quantum critical point due to Kondo and RKKY competition. The presence of magnetic anisotropy and alloy disorder leads to the formation of a Griffiths phase with giant spins in magnetic clusters. Low-energy excitations result from the tunnelling of spins over classically forbidden regions. Predictions for the temperature dependence of the specific heat, magnetic susceptibility and other thermodynamic functions are given in terms of an exponent λ:

$$\frac{C}{T} \propto \chi(T) \propto T^{\lambda-1}. \tag{13}$$

Experimentally [41] it is found that the $C(T)$ data for $UCu_{5-x}Pd_x$, UCu_4Pt, $U_{1-x}Y_xPd_3$ and $U_{1-x}Th_xPd_2Al_3$ agree with the prediction of (13) at low temperatures with λ-values ranging from 0.7 to 0.85. For $U_{0.6}Th_{0.4}Pd_2Al_3$, the $C(T)$ data give $\lambda = 0.84$ while the $\chi(T)$ data give $\lambda = 0.63$ for the same alloy. In view of our observed power-law behaviour of $\chi(T)$ for sufficiently small fields, we find, in terms of (13), $\lambda = 0.345 \pm 0.005$ for $x = 0.7$ and $\lambda = 0.420 \pm 0.005$ for $x = 0.8$. These are lower than the values obtained by de Andrade *et al* [41], but we note the strong dependence of the low-temperature slope in figure 17 on the field strength. De Andrade *et al* [41] used applied fields between 0.5 and 1 T in their studies which has to lead to a smaller slope of $\log \chi(T)/\log T$ and thus to larger values of λ. Comparison of our different isofield curves depicted in figure 17 gives confidence that the power-law behaviour observed for the smallest field of $B = 0.008$ T presents a reliable value of m (and hence λ) in the low-field limit.

A field-dependent susceptibility could also originate from a Kondo-disorder model [19,47,53]. In this case there will be a finite number of uncompensated spins at low temperature and these could impart a saturating behaviour to M/B in higher magnetic fields which would not be the case if the Kondo ions are homogeneously screened. On the basis of results from conformal field theory [54] and the observed energy dependence of inelastic neutron scattering data, Aronson *et al* [55] were able to describe their $\chi(T)$ data for NFL $UCu_{5-x}Pd_x$ ($x = 1$, 1.5) using a $\chi \sim T^{-m}$ power law with $m = \frac{1}{3}$. Our $\chi(T)$ data for the NFL $U_{1-x}Th_xPd_2Al_3$ system for $T \to 0$, $B \to 0$ depicted in figure 17 indicate a more rapid temperature variation than that found by Aronson *et al* for $UCu_{5-x}Pd_x$.

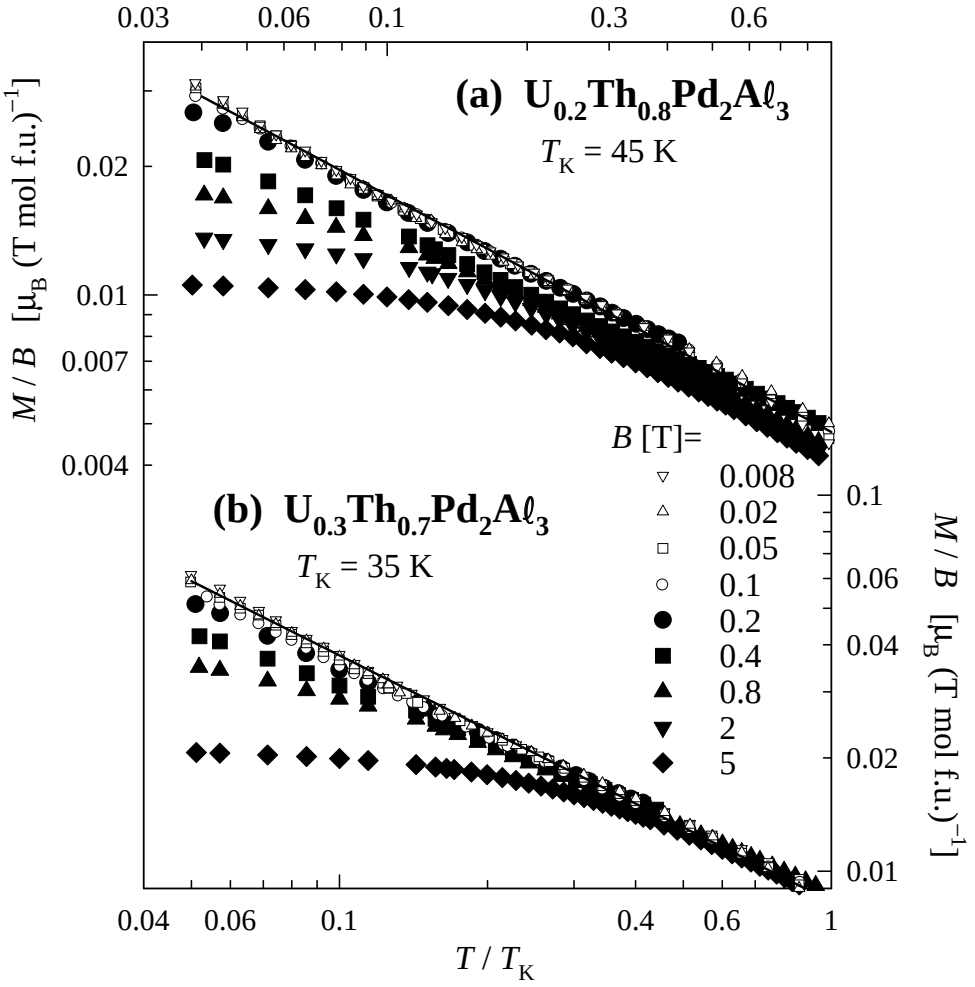

Figure 17. A comparison in a double-$\log_{10}$ plot of the magnetic susceptibility $\chi(T) = M(B)/B$ for (a) $U_{0.2}Th_{0.8}Pd_2Al_3$ and (b) $U_{0.3}Th_{0.7}Pd_2Al_3$ using various measuring fields. The solid lines superimposed onto the data at the lowest field values for both compounds are obtained by a power-law fit to the $1.7 \leqslant T \lesssim 40$ K data, with parameters as given in the text.

4. Conclusions

A study of the magnetic, Kondo and NFL behaviour of the $U_{1-x}Th_xPd_2Al_3$ system, using magnetization, resistivity and MR measurements, has been reported. The magnetic phase diagram determined earlier by Maple *et al* is largely confirmed in our study. Zero-field resistivity measurements indicate NFL behaviour at low temperature for compounds with $0.4 \leqslant x \leqslant 0.7$ over more than one decade of temperature. However, at the lowest temperatures a departure from the NFL behaviour takes place. Furthermore, application of large magnetic fields (up to 14 T) recovers FL dynamics. Magnetoresistance measurements are described in single-ion terms using the Bethe-*ansatz* solution of the Coqblin–Schrieffer Hamiltonian. This yields values of the Kondo temperature T_K and a considerably reduced effective moment μ_K of the Kondo ion. Non-linear magnetization-versus-field curves are observed for samples

in the NFL region. We show that these $M(B)$ curves agree with the expectations from the two-channel Kondo model for low fields. It is noted that the exponent n that is observed in the scaling-law expression for the resistivity takes on values of $n \approx 1$ for $U_{1-x}Th_xPd_2Al_3$ alloys in the NFL region. Such values are intermediate between the expectations [18, 56] at low temperature for the conventional single-channel Kondo effect ($n = 2$) and for the two-channel spin-$\frac{1}{2}$ Kondo effect ($n = \frac{1}{2}$). Thus, whereas the magnetic response suggests the applicability of a two-channel Kondo model, this model is not supported by the resistivity results. It would be of interest to extend the magnetization and susceptibility studies to lower temperatures in order to ascertain whether the scaling laws found in our work extend to such temperatures. More detailed investigations using a variety of experimental probes and preferably single-crystal specimens of the NFL compositions are furthermore required for a more complete comparison with the various theoretical descriptions.

Acknowledgments

Financial support by the South African National Research Foundation and by the University of the Witwatersrand Research Committee is acknowledged. The work at the W Trzebiatowski Institute of Low Temperature and Structure Research, Wrocław, was supported by the State Committee for Scientific Research in Poland within Grant No 2P03B14710. Mr R Gorzelniak is thanked for valued technical assistance.

References

[1] Geibel C, Schank C, Thies S, Kitazawa H, Bredl C D, Böhm A, Rau M, Grauel A, Caspary R, Helfrich R, Ahlheim U, Weber G and Steglich F 1991 *Z. Phys.* B **84** 1
[2] Krimmel A, Loidl A, Fischer P, Roessli B, Dönni A, Kita H, Sato N, Endoh Y, Komatsubara T, Geibel C and Steglich F 1993 *Solid State Commun.* **87** 829
[3] Kita H, Dönni A, Endoh Y, Kakurai K, Sato N and Komatsubara T 1994 *J. Phys. Soc. Japan* **63** 726
[4] Feyerherm R, Amato A, Gygax F N, Schenck A, Geibel C, Steglich F, Sato N and Komatsubara T 1994 *Phys. Rev. Lett.* **73** 1849
[5] Amato A 1997 *Rev. Mod. Phys.* **69** 1119
[6] Krimmel A, Fischer P, Roessli B, Maletta H, Geibel C, Schank C, Grauel A, Loidl A and Steglich F 1992 *Z. Phys.* B **86** 161
[7] Grauel A, Böhm A, Fischer H, Geibel C, Köhler R, Modler R, Schank C, Steglich F, Weber G, Komatsubara T and Sato N 1992 *Phys. Rev.* B **46** 5818
[8] Paolasini L, Paixão L A, Lander G H, Burlet P, Sato N and Komatsubara T 1994 *Phys. Rev.* B **49** 7072
[9] Oda K, Kumada T, Sugiyama K, Sato N, Komatsubara T and Date M 1994 *J. Phys. Soc. Japan* **63** 3115
[10] Dalichaouch Y and Maple M B 1994 *Physica* B **199+200** 176
[11] Maple M B, Seaman C L, Gajewski D A, Dalichaouch Y, Barbetta V B, de Andrade M C, Mook H A, Lukefahr H G, Bernal O O and MacLaughlin D E 1994 *J. Low Temp. Phys.* **95** 225
[12] Maple M B, de Andrade M C, Herrmann J, Dalichaouch Y, Gajewski D A, Seaman C L, Chau R, Movshovich R, Aronson M C and Osborn R 1995 *J. Low Temp. Phys.* **99** 223
[13] Maple M B, Dalichaouch Y, de Andrade M C, Dilley N R, Herrmann J and Movshovich R 1995 *J. Phys. Chem. Solids* **56** 1963
[14] Maple M B, Dickey R P, Herrmann J, de Andrade M C, Freeman E J, Gajewski D A and Chau R 1996 *J. Phys.: Condens. Matter* **8** 9773
[15] Moriya T and Takimoto T 1995 *J. Phys. Soc. Japan* **64** 960
[16] Sengupta A M and Georges A 1995 *Phys. Rev.* B **52** 10 295
[17] Schlottmann P and Sacramento P D 1993 *Adv. Phys.* **42** 641
[18] Cox D L and Zawadowski A 1998 *Adv. Phys.* **47** 599
[19] Bernal O O, MacLaughlin D E, Lukefahr H G and Andraka B 1995 *Phys. Rev. Lett.* **75** 2023
[20] Castro Neto A H, Castilla G and Jones B A 1998 *Phys. Rev. Lett.* **81** 3531
[21] du Plessis P de V, Strydom A M and Gers R P 1997 *Physica* B **230–232** 610
[22] Andrei N 1982 *Phys. Lett.* A **87** 299

[23] Schlottmann P 1983 *Z. Phys.* B **51** 223
[24] Miranda E, Dobrosavljević V and Kotliar G 1996 *J. Phys.: Condens. Matter* **8** 9871
[25] Dalichaouch Y, de Andrade M C and Maple M B 1992 *Phys. Rev.* B **46** 8671
[26] Sato N, Sakon T, Takeda N, Komatsubara T, Geibel C and Steglich F 1992 *J. Phys. Soc. Japan* **61** 32
[27] Bakker K, de Visser A, Tai L T, Menovsky A A and Franse J J M 1993 *Solid State Commun.* **86** 497
[28] Huth M, Kaldowski A, Hessert J, Steinborn T H and Adrian H 1993 *Solid State Commun.* **87** 1133
[29] Sato N, Aso N, Hirota K, Komatsubara T, Endoh Y, Shapiro S M, Lander G H and Kakurai K 1996 *Phys. Rev.* B **53** 14 043
[30] Hessel Andersen N 1980 *Crystalline Electric Field and Structural Effects in f-Electron Systems* ed J E Crow, R P Guertin and T W Mihalisin (New York: Plenum) p 373
[31] Petersen T, Mason T E, Aeppli G, Ramirez A P, Bucher E and Kleiman R N 1994 *Physica* B **199+200** 151
[32] Sato N, Aso N, Lander G H, Roessli B, Komatsubara T and Endoh Y 1997 *J. Phys. Soc. Japan* **66** 1884
[33] Metoki N, Haga Y, Koike Y, Aso N and Ōnuki Y 1997 *J. Phys. Soc. Japan* **66** 2560
[34] Blatt F J 1968 *Physics of Electronic Conduction in Solids* (New York: McGraw-Hill)
[35] Strydom A M, du Plessis P de V and Gridin V V 1996 *Physica* B **225** 89
[36] Bloomfield P E, Hecht R and Sievert P R 1970 *Phys. Rev.* B **2** 3714
Ruvalds J and Sheng Q G 1988 *Phys. Rev.* B **37** 1959
Tian D P and Keiter H 1993 *Solid State Commun.* **87** 813
[37] Felsch W and Winzer K 1973 *Solid State Commun.* **13** 569
Remenyi G, Jaccard D, Flouquet J, Briggs A, Fisk Z, Smith J L and Ott H R 1986 *J. Physique* **47** 367
Thompson J D, McElfresh M W, Willis J O, Fisk Z, Smith J L and Maple M B 1987 *Phys. Rev.* B **35** 48
Strydom AM and du Plessis P de V 1999 *J. Phys.: Condens. Matter* **11** 2285
[38] Andrei N, Furuya K and Lowenstein J H 1983 *Rev. Mod. Phys.* **55** 331
[39] Huth M, Hessert J, Jourdan M, Kaldowski A and Adrian H 1994 *Phys. Rev.* B **50** 1309
[40] Batlogg B, Bishop D J, Bucher E, Golding B Jr, Ramirez A P, Fisk Z, Smith J L and Ott H R 1987 *J. Magn. Magn. Mater.* **63+64** 441
[41] de Andrade M C, Chau R, Dickey R P, Dilley N R, Freeman E J, Gajewski D A, Maple M B, Movshovich R, Castro Neto A H, Castilla G E and Jones B A 1998 *Phys. Rev. Lett* **81** 5620
[42] Strydom A M, du Plessis P de V and Troć R 1999 *Physica* B **259–261** 421
[43] Ramirez A P, Chandra P, Coleman P, Fisk Z, Smith J L and Ott H R 1994 *Phys. Rev. Lett.* **73** 3018
[44] Aliev F G, Vieira S, Villar R and Moshchalkov V V 1996 *J. Phys.: Condens. Matter* **8** 9807
[45] Gajewski D A, Dilley N R, Chau R and Maple M B 1996 *J. Phys.: Condens. Matter* **8** 9793
[46] Lukefahr H G, Bernal O O, MacLaughlin D E, Seaman C L, Maple M B and Andraka B 1995 *Phys. Rev.* B **52** 3038
[47] MacLaughlin D E, Bernal O O and Lukefahr H G 1996 *J. Phys.: Condens. Matter* **8** 9855
[48] Vollmer R, Mock S, Pietrus T, von Löhneysen H, Chau R and Maple M B 1997 *Physica* B **230–232** 603
[49] du Plessis P de V, Strydom A M, Cichorek T, Troć R and Levin E M 1998 *J. Magn. Magn. Mater.* **177–181** 457
[50] von Löhneysen H, Pietrus T, Portisch G, Schlager H G, Schröder A, Sieck M and Trappmann T 1994 *Phys. Rev. Lett.* **72** 3262
[51] Nozières P and Blandin A 1980 *J. Physique* **41** 193
[52] Morin P and Schmitt D 1981 *Phys. Rev.* B **23** 5936
[53] Bernal O O, MacLaughlin D E, Amato A, Feyerherm R, Gygax F N, Schenck A, Heffner R H, Le L P, Nieuwenhuys G J, Andraka B, von Löhneysen H, Stockert O and Ott H R 1996 *Phys. Rev.* B **54** 13 000
[54] Affleck I and Ludwig A W W 1993 *Phys. Rev.* B **48** 7297
[55] Aronson M C, Maple M B, Chau R, Georges A, Tsvelik A M and Osborn R 1996 *J. Phys.: Condens. Matter* **8** 9815
[56] Ludwig A W W 1994 *Physica* B **199+200** 406